Radioelectronic and Computer Systems, 2025, no. 2(114)
ISSN 1814-4225 (print)
ISSN 2663-2012 (online)

UDC 004.942: 614:4
doi: 10.32620/reks.2025.2.05

Dmytro CHUMACHENKO[1, 2, 3]

[1]*National Aerospace University "Kharkiv Aviation Institute", Kharkiv, Ukraine*
[2]*Balsillie School of International Affairs, Waterloo, ON, Canada*
[3]*University of Waterloo, Waterloo, ON, Canada*

EXPERIMENTAL STUDY ON PREPAREDNESS OF DISEASE X WITH AN AGENT-BASED FRAMEWORK SCENARIO-DRIVEN ANALYSIS

Emerging respiratory pathogens continue to impose substantial health and economic burdens worldwide, motivating generic readiness tools that do not rely on pathogen-specific data. This study investigates how five archetypal stressors, namely, rising antivaccine misinformation, behavioural fatigue, vaccine supply disruption, immune escape variant emergence, and armed conflict infrastructure collapse, reshape the course of a hypothetical high-consequence agent designated Disease X. The study's objective is to quantify each shock's epidemiological impact in an otherwise identical urban population and to identify the systemic vulnerabilities that most threaten early outbreak control. Addressing that objective required the following tasks, which began with a critical review of scenario-based epidemic modelling, progressed to the extension of a validated SEIRDV agent-based core with dynamic belief diffusion, dose-queue logistics, and conflict-driven mobility, and provided experiments per scenario using parameters anchored in peer-reviewed evidence. The framework shows that a 15% point surge in antivaccine belief doubles the peak prevalence and adds 258 deaths. A 50-point erosion of masking and distancing produces a secondary wave that still trims by 9% after fatigue re-engagement. A 70 % mRNA supply shortfall lasting 35 days increases deaths by 7%, and seeding 50 immune-escape cases (R0≈9.5, 60 % neutralization loss) increases cumulative mortality by 41 % within six weeks. The composite conflict shock elevates deaths by 71 % despite a 10% population outflow. These non-linear responses arise solely from changes in behaviour, logistics, or context, as biological constants remain fixed. The findings demonstrate that preparedness cannot rely on any single lever. Effective mitigation demands synchronized risk communication, staged behavioural support, diversified and buffered manufacturing capacity, rapid antigenic update pathways and humanitarian vaccination corridors. This study supplies a decision support instrument for stress-testing policy portfolios before the next high-consequence outbreak.

Keywords: *epidemic model; epidemic process; epidemic simulation; simulation; agent-based simulation; misinformation; vaccine hesitancy; disease X.*

1. Introduction

Emerging and re-emerging infectious diseases remain a principal source of global morbidity, mortality, and economic disruption. The annual catalogue of high-impact events, from successive Ebola flare-ups to the SARS-CoV-2 pandemic, demonstrates that zoonotic spillover is neither rare nor self-limiting, and respiratory pathogens, in particular, can trigger cascades that overwhelm even high-income health systems [1]. In response, governments and multilateral agencies are negotiating a pandemic prevention treaty to codify surveillance, data sharing, and countermeasure equity before the next crisis unfolds [2].

Mathematical and computational simulation has become indispensable to this preparedness agenda because it affords an ethically unobjectionable, rapidly iterated means of probing interventions that cannot be randomized in vivo [3]. Agent-based models (ABMs) are particularly valuable because they represent individuals and their heterogeneous contact patterns. They capture superspreading, behavioural feedback, and logistical bottlenecks that ordinary compartmental differential equation models abstract away. Recent ABM applications have ranged from facility-level ventilation studies [4] to city-scale hybrid simulations integrating stochastic transmission with healthcare resource modules [5], demonstrating that explicit context representation can materially change policy rankings.

Against this background, the World Health Organization (WHO) introduced the placeholder "Disease X", also termed "Pathogen X", to denote a future, as-yet-unidentified agent with epidemic or pandemic potential [6]. Decoupling preparedness research from any single microbe encourages generic capability building, flexible manufacturing platforms, plug-and-play trial protocols, and modelling frameworks that can be swiftly refitted to the pathogen that ultimately emerges. Recent revisions of the WHO priority pathogen list reiterate the need for Disease X scenario planning and

emphasize the role of quantitative simulation in stress-testing response options before the window for containment closes [7].

This paper contributes to that effort by deploying a high-resolution ABM, previously formalized and validated in [8], to examine five archetypal stressors, behavioural, sociological, logistical, virological, and geopolitical, that could modulate the course of a Disease X outbreak.

The effect of each perturbation on attack rates, vaccination coverage, and fatality burden was quantified through counterfactual experimentation under identical biological assumptions. By grounding scenario parameters in recent empirical reports, the study seeks to provide a transferable template for rapid decision support once the next "unknown" pathogen moves from abstraction to reality.

The primary **objective** of this study is to evaluate how five qualitatively distinct exogenous stressors can reshape the trajectory of a hypothetical high-consequence respiratory pathogen ("Disease X") when it encounters a demographically realistic, behaviourally heterogeneous urban population. The overarching aim of this study is to generate actionable insights for preparedness planners by identifying the systemic vulnerabilities that most threaten epidemic control in the early months of an as-yet-unknown outbreak.

To achieve this objective, the following **tasks** were formulated:

1. To comprehensively review existing scenario-based models for the simulation of infectious diseases.

2. To develop an experimental setting that reflects five scenarios based on real-world parameters.

3. To provide an experimental study of the Disease X simulation under five scenarios.

4. To analyze the experimental study results.

This study contributes to research on pandemic preparedness simulation in two ways. Firstly, a previously validated ABM was extended to accommodate Disease X-specific natural history and embed three interacting subsystems, offering a transparent stand-alone framework that can be re-parameterized for future pathogens. Secondly, the five experimental conditions are parameterized with empirical evidence from 2019-2025 events, including documented vaccine-supply bottlenecks, Omicron immune escape, and health system degradation during the Russian full-scale invasion of Ukraine.

Section 2 (Current Research Analysis) provides a comprehensive review of recent scenario-based modelling studies in the context of infectious disease simulation, emphasizing the advances and limitations in behavioural response modelling. Section 3 (Methodology) details the structure and logic of the proposed ABM framework and the experimental study concept. Section 4 (Experimental Results) applies the model to the spread of Disease X under five scenarios. Section 5 (Discussion) interprets the results and identifies implications for pandemic preparedness and communication strategy. Finally, the Conclusions summarize the theoretical and practical contributions of the paper and outline directions for future research.

The current research is part of a comprehensive information system for assessing the impact of emergencies on the spread of infectious diseases [9].

2. Current Research Analysis

Recent research on epidemic modelling exhibits a marked pluralism of methods, with studies deploying large-scale agent-based simulations, age-stratified compartmental systems, metapopulation pipelines, machine learning surrogates and reinforcement learning controllers to interrogate transmission dynamics, health system demand, and policy effectiveness. Common threads include increasingly fine-grained calibration to mobility and clinical surveillance data, explicit behavioural or economic feedback treatment, and scenario ensembles to inform real-time decision-making. This study demonstrates that state-of-the-art models combine heterogeneous data streams with high-performance computation to deliver operational projections. However, each contribution addresses only a subset of the complex couplings that shape pandemic risk.

The study by Devaux et al. [10] interrogated the long-term burden of non-communicable diseases (NCDs) in Europe by embedding expert-derived qualitative foresight narratives into a microsimulation platform that tracks demographic change, five behavioural risk factors, and multi-disease morbidity until 2050. Their framework generates a business-as-usual trajectory, two optimistic "response" visions that assume coordinated policy action, and one pessimistic storyline characterized by economic recession and widening inequity. These four narratives are benchmarked against stylized best- and worst-case risk-factor envelopes. The results indicate that population aging is the dominant driver of NCD incidents. However, variations in future smoking, alcohol use, obesity, inactivity, and hypertension still shift life-expectancy forecasts by up to four years and premature mortality trends by as much as nine percentage points across scenarios. The authors conclude that structural policies capable of bending risk-factor curves, particularly those targeting obesity and hypertension, are essential if Europe is to realize the Sustainable Development Goal of a one-third reduction in premature NCD deaths by 2030.

Groves-Kirkby et al. [11] presented a national-scale implementation of OpenABM-COVID-19 for England, embedding a bespoke software wrapper that automates

ISSN 1814-4225 (print)
ISSN 2663-2012 (online)

daily calibration of key transmission and clinical parameters to three National Health Service (NHS) operational data streams (hospital admissions, ICU occupancy, and deaths). The fitted model is propagated forward to produce decision-grade projections of clinical demand. The calibration combines a two-stage grid search for biologically salient parameters with geography-specific tuning of transmission multipliers, enabling stable fits across 42 Integrated Care Systems while keeping computation tractable on Azure Batch infrastructure. The calibrated model reproduces temporal and regional infection dynamics, as confirmed by cross-validation against independent incidence estimates. Once calibrated, the framework generates scenario ensembles that inform NHS operational planning: winter-2020 lockdown options, vaccine-rollout effects, and roadmap easing, each produced within 48 h of policy announcements and disseminated to downstream analytics pipelines through the NHS COVID-19 Data Store. The authors argue that large-scale, data-linked ABMs bridge the gap between academic modelling and real-time healthcare decision support, highlighting the importance of open-source code, reproducible pipelines, and granular health system data integration.

Ndefru et al. [12] presented CoviDeS, a city-scale risk-informed decision-support tool that couples a mechanistic SIRD agent-based simulator with a dynamic Bayesian network (DBN) tuned such that uncertain behavioural inputs, such as mask adherence, testing uptake, mobility, and vaccine acceptance, propagate through explicitly probabilistic nodes and influence transmission, severity, and healthcare utilization. The prototype is parameterized for Los Angeles, calibrated to public incidence and hospital data, and then exercised on policy cases ranging from university reopening to phased vaccine rollout and universal masking, thereby illustrating how the DBN layer exposes the causal pathways linking interventions to epidemic outcomes and how the integrated platform can be run fast enough to inform real-time local decisions.

Estill et al. [13] developed an age-stratified stochastic compartmental model of SARS-CoV-2 transmission in Switzerland that partitions the population into children (0–17 years), adults (18–64 years), and seniors (≥ 65 years). They calibrated disease progression parameters, baseline infectiousness, and contact matrices to canton-level hospitalization and mortality data before projecting epidemic dynamics to December 2020 under alternative post-lock-down contact-reduction strategies. The analysis compares a business-as-usual relaxation with six counterfactuals ranging from full eradication through 76 % uniform contact suppression to targeted or “start-stop” interventions that modulate contacts by age or trigger renewed lockdowns when hospital admissions exceed thresholds. Outputs from 1 000 Monte-Carlo realizations provide credible intervals for daily deaths, intensive care unit (ICU) occupancy, and cumulative infections. Results indicate that at least a 54 % across-the-board contact reduction is required to keep ICU demand below the national capacity of 1 200 beds, while age-focused restrictions or partial measures permit epidemic rebound as early as July. Full eradication is achievable only with ≥ 76 % contact suppression, yet leaves the population largely immunologically naïve. The authors conclude that sustained, population-wide distancing remains essential until vaccine rollout and that reactive “start-stop” lockdowns would entail multiple prolonged closures within the year, although epidemiologically effective.

Chinazzi et al. [14] described a multiscale, age-structured, multi-strain metapopulation framework that couples the Global Epidemic and Mobility model (GLEAM) with a county-resolved Local Epidemic and Mobility model for the United States (LEAM-US). The framework generates state- and national-level projections for cases, hospitalizations, and deaths under the Scenario Modeling Hub (SMH) specification set. The platform integrates international and domestic air traffic data, county commuting flows, Google mobility indicators, OxCGRT policy indices, and CDC vaccination series. It calibrates epidemiological and severity parameters via approximate Bayesian computation against hospital-death time series and mechanistically seeds novel variants through importations simulated in GLEAM, whose outputs initialize LEAM-US to capture spatial heterogeneity in strain competition, vaccination, and non-pharmaceutical-intervention dynamics. A case study on the Alpha (B.1.1.7) wave shows the model reproducing the staggered rise to dominance across 3 142 counties, explains the effective reproduction number uplift via importation timing and local contact patterns, and matches weighted interval score benchmarks when compared with CDC ensemble forecasts, thus illustrating how coordinated scenario pipelines can provide federal and state planners with decision-grade situational awareness.

López and Rodó [15] developed an extended SEIR model that adds a protection (confinement) compartment P and a presymptomatic infectious stage to capture behavioural countermeasures during the first COVID-19 wave in Spain and Italy. Model parameters are estimated by nonlinear least squares against nationally aggregated cases, recoveries, and deaths and are later down-scaled to Spain’s 17 autonomous communities to explore sub-national heterogeneity. After calibration, the authors conduct counterfactual simulations that raise or lower the protection rate to emulate earlier, later, stricter, or milder stay-at-home orders. The results reveal that doubling the protection rate would have delayed and flattened the epidemic peak by several weeks. In contrast, a 10-fold increase could have reduced the number of peak infections from >1.4 million to ≈ 100 000 and halved cumulative deaths. This study illustrates how simple structural

extensions to classical compartmental models can quantify the time sensitivity of NPI and inform rapid-response policy during rapidly unfolding outbreaks.

Sun et al. [16] investigated spatial and temporal heterogeneity in COVID-19 mortality across the continental United States by replacing classical compartmental dynamics with a Geographically and Temporally Neural-Network Weighted Regression (GTNNWR) framework that learns non-stationary relationships between deaths and a suite of epidemiological covariates at the county level. The authors trained the model on weekly mortality, vaccination, mobility, and mask-use data from March 2020 to February 2023. They compared GTNNWR's predictive skill with a baseline age-stratified SEIR implementation and showed that GTNNWR lowers the mean absolute percentage error by roughly nine points while revealing pronounced regional differences in intervention efficacy. The fitted model was then driven through five counterfactual intervention pathways to quantify prospective death reductions under each strategy. Results indicate that universal masking yields the largest single-measure benefit (−5.4 % deaths nationwide), that vaccine acceleration alone achieves a smaller but meaningful reduction (−3.6 %), and that simultaneous deployment of all three interventions would cut cumulative fatalities by 27 % overall and up to 45 % during winter surges, underscoring the importance of layered, coordinated mitigation.

Qin et al. [17] developed a reinforcement learning (RL) decision-support platform that recommends NPI schedules to mitigate seasonal influenza transmission in mainland China while limiting economic disruption. The authors embed a deep-Q-network (DQN) agent within an empirically parameterized SIR simulator calibrated with weekly surveillance data from 2019 to 2023 and augmented with labour-force participation weights to approximate gross domestic product losses. To address the skewed state distribution characteristic of long epidemic rollouts, a variance-weighted replay buffer was introduced that preferentially samples rare but high-impact epidemiological states during training, accelerating convergence and improving policy robustness. The trained RL agent was benchmarked against heuristic fixed-threshold and proportional-control policies across six spatiotemporal settings that captured the pre-, intra-, and post-COVID-19 periods in the northern and southern influenza transmission zones. Simulation experiments show that the enhanced DQN lowers cumulative infections by 3-6 % and reduces combined health-economic loss by approximately 2.8 % relative to a vanilla DQN and by larger margins relative to heuristic baselines, highlighting the promise of adaptive, data-driven NPI scheduling for endemic respiratory pathogens.

Gandzha, Kliushnichenko, and Lukyanets [18] expanded the classical susceptible-infectious-recovered paradigm by constructing a five-compartment susceptible-infectious-recovered (SIQR) model that explicitly separates quarantined individuals from free-circulating infective and adds an environmental cloud variable to capture indirect transmission via contaminated media. Analytic expressions for all rate constants regarding socially adjustable factors are derived, thereby linking epidemiological dynamics to concrete behavioural levers. An Arrhenius-like resource-recovery term is another innovation in which the clinical recovery rate accelerates with per-capita economic output, creating feedback between epidemic control and macroeconomic capacity. Calibration to stylized COVID-19 parameters allows systematic exploration of mobility restrictions, quarantine timing, surface disinfection, and income-support policies. Numerical experiments reveal strong nonlinear synergies, showing, for example, that modest contact rate reductions coupled with financial support can outperform stringent but resource-starved lockdowns in health and economic metrics. Thus, this study illustrates how integrating indirect transmission and resource constraints yields richer insight into optimal intervention portfolios than classical SIR formulations.

Gao and Wang [19] proposed a two-layer decision support architecture that couples an average-field SIR network model with a DBN that translates those markers, together with expert-elicited probabilities for alternative interventions, into an integrated cost-benefit ranking of response plans. The infectious disease dynamics layer was calibrated to national and Wuhan COVID-19 surveillance series, reproducing observed case and death trajectories with narrow uncertainty envelopes ($R_0 \approx 1.5$–1.7). Outputs from the calibrated dynamics feed the scenario nodes of the DBN, where three candidate policies differing in quarantine stringency and surge capacity investment are evaluated through a cumulative foreground utility function that jointly scores epidemiological and economic performance. Sensitivity analysis shows that a moderate contact reduction strategy supplemented by additional medical resources consistently minimizes infections, shortens epidemic duration, and yields the highest cost-benefit ratio.

A summary of the scenario-based epidemic models is presented in Table 1. The framework developed in this study synthesizes these strands by embedding behavioural misinformation diffusion, supply-chain-aware vaccination logistics, and conflict-induced mobility shocks within a single agent-based SEIRDV architecture calibrated for a pathogen-agnostic Disease X. The platform enables counterfactual stress tests that quantify the marginal and joint impacts of disinformation, fatigue, manufacturing disruption, immune escape, and armed conflict by unifying modules that have been explored in isolation.

ISSN 1814-4225 (print)
ISSN 2663-2012 (online)

Table 1

The current state of scenario-based epidemic models

Paper	Task	Approach	Scenarios	Findings
Devaux M. et al. [10]	This study quantifies how Europe's NCD burden will evolve to 2050 under alternative assumptions about five behavioural risk factors.	Horizon-scanning narratives are integrated with a microsimulation that projects age-, sex-, and region-specific disease and mortality outcomes from 2015 to 2050.	Four main narratives, namely, business-as-usual ("The Rich Get Healthier"), two optimistic responses ("We Will Health You", "Healthy Together"), and one pessimistic ("Desolation Health"), are benchmarked against stylized best- and worst-case risk factor envelopes.	Population aging remains the dominant driver, but optimistic risk trajectories delay disease onset and increase life expectancy by up to four years. In contrast, the pessimistic path shifts morbidity to working-age adults and halts the reduction of premature mortality.
Groves-Kirkby N. et al. [11]	Quantification of future hospital care demand for COVID-19 in England by calibrating and running an ABM at the national population scale.	Integrates Open-ABM-COVID-19 with the specific pipeline to automate the daily calibration of NHS SitRep data and forward simulation under varying policy and vaccination assumptions.	Baseline and counterfactual trajectories covering winter 2020 lockdowns, staged reopening, vaccination rollout, and sensitivity analyses on transmission and behaviorr were evaluated.	Calibrated simulations closely match unseen incidence data and provide timely, geographically resolved projections that guide NHS capacity planning during successive pandemic waves.
Ndefru B. et al. [12]	The community-level impact of alternative COVID-19 policies under behavioural and epidemiological uncertainty was quantified.	Embed a DBN of behavioural variables around a SIRD agent-based simulator, calibrating the hybrid model to Los Angeles data.	The test cases include campus reopening, staged vaccination strategies, and a hypothetical 100 % mask mandate.	Rapid single-dose coverage combined with universal masking yields the largest reduction in infections and hospital demand, outperforming slower two-dose schedules or no masking.
Estill J. et al. [13]	Quantify how differing levels and patterns of post-lockdown contact reduction will shape the trajectory of the COVID-19 epidemic in Switzerland through December 2020.	Applying a three-age-group stochastic compartmental model calibrated to Swiss hospitalizations and deaths, then simulate 1 000 Monte-Carlo realizations for each intervention strategy.	Baseline relaxation plus six counterfactuals: uniform eradication (76 % cut), epidemic control (54 % cut), three age-targeted reductions, and a threshold-triggered start-stop lockdown strategy.	Uniform contact cuts of ≥ 54 % keep ICU demand below capacity, and 76% eradicate the epidemic by July, whereas age-focused or lighter measures permit early rebound and larger autumn waves.
Chinazzi M. et al. [14]	Deliver SMH-compliant projections of COVID-19 cases, hospitalizations, and deaths in the United States, with explicit characterization of variant emergence and spatial heterogeneity.	Couple GLEAM-based international seeding with a county-level, age-structured LEAM-US metapopulation model calibrated by ABC to surveillance deaths and hospital data.	Implement four SMH Round 5 scenarios that vary vaccination uptake (high 83 % vs low 68 %) and NPI relaxation (moderate 50 % vs low 80 %).	The model captures substantial interstate and intrastate variations in the dominance of the Alpha-variant and accurately projects ICU demand, outperforming naïve baselines while matching the skill metrics of the ensemble forecast.

Continuation of the Table 1

Paper	Task	Approach	Scenarios	Findings
López L. and Rodó X. [15]	Estimate Spain's and Italy's first-wave COVID-19 dynamics and quantify how alternative confinement intensities and timings would alter epidemic peaks and deaths.	Fit a modified SEIR model with presymptomatic and protection compartments to national and regional data, then run stochastic simulations under varying daily protection rates.	The observed trajectory is compared with counterfactual cases that double, triple, or decrease the protection rate and with delays of up to several days in lockdown onset.	Stricter or earlier confinement substantially lowers and delays epidemic peaks, resulting in up to a 10-fold reduction in infections and ~50 % fewer deaths, whereas even brief implementation delays markedly worsen outcomes.
Sun J. et al. [16]	Estimate county-level COVID-19 deaths and quantify the mortality benefits of alternative mask, distancing, and vaccination strategies across the United States.	A GTNNWR model was calibrated on weekly mortality and intervention covariates, benchmarked against a baseline SEIR, and propagated under counterfactual inputs.	Five scenarios were evaluated: observed status quo, universal masking, intensified distancing, accelerated vaccination, and a combined high-intensity package.	GTNNWR outperforms SEIR. Masks alone reduce deaths by 5.4 %, vaccination by 3.6 %, and distancing by 2.7 %, and the combined package achieves a 27 % nationwide reduction (≥ 45 % in winter waves).
Qin X. et al. [17]	Design an RL system that selects NPI intensities to minimize the joint health and economic burden of seasonal influenza in China.	Train a deep Q-network with a variance-weighted replay buffer inside a surveillance-calibrated SIR simulator covering 2019-2023.	We evaluated six settings defined by region (north vs south) and epidemic era (pre-COVID, COVID, and post-COVID).	The enhanced DQN outperforms the heuristic and vanilla-DQN baselines, cutting infections and lowering the combined loss by ≈ 2.8 % across all scenarios.
Gandzha I.S., Kliushnichenko O.V., Lukyanets S.P. [18]	To capture the joint effects of direct and indirect transmission and economic resources on epidemic dynamics.	A five-compartment SIQR model with an environmental cloud and an Arrhenius-type resource recovery feedback, parameterized by controllable social contact variables, is developed.	Comparison of baseline mobility, soft- and strict quarantine regimes, and resource limitation cases that curtail medical capacity.	Indirect transmission and depleted resources can increase fatalities by an order of magnitude, whereas moderate contact cuts and economic support flatten infection and death curves.
Gao S., Wang H. [19]	Develop a modelling system that predicts epidemic trajectories and ranks COVID-19 emergency response options for COVID-19 in China.	Couple an average field SIR network calibrated to surveillance data with a DBN that evaluates intervention portfolios via a cost-benefit utility metric.	Analyze six epidemic stages under three policy options that vary quarantine strictness and medical resource deployment.	The integrated IDD–DBN framework fits observed data and identifies a moderate quarantine, resource-supported policy as the optimal balance between health protection and economic cost.

3. Methodology

3.1. Modelling Framework

The experimental study simulates Disease X, a notional severe-acute respiratory infection designated by the World Health Organization as a prototype for future pandemic threats [20]. The spread of Disease X was simulated in the multilayer agent-based architecture developed in [8], adapting that framework to the pathogen's putative natural history while leaving its logical structure unchanged.

A discrete-time SEIRDV engine is at the base. Each agent occupies one of six mutually exclusive

ISSN 1814-4225 (print)
ISSN 2663-2012 (online)

compartments (susceptible (S), exposed (E), infectious (I), recovered (R), vaccinated (V), or deceased (D)) and attempts one Bernoulli transition per day. The transition probabilities were calculated from the canonical parameters β (per-contact transmissibility), σ (latency inverse), γ (infectious- period inverse), and μ (fatality rate). For Disease X, the reference scenario adopts $\sigma^{-1} = 3.3$ days, $\gamma^{-1} = 7$ days, and an initial basic reproduction number $R_0 \approx 7$, values aligned with the upper-quartile estimates for recent high-transmission coronaviruses. All transmission occurs along a Watts–Strogatz small-world graph (average degree = 15 and rewiring probability = 0.1), yielding realistic clustering and short global path lengths [21].

The three auxiliary layers complete the model. First, a behavioural module endows every agent with a vaccination-willingness score that is dynamically influenced by personal misinformation exposure, peer signals, and scenario-specific shocks. Willingness translates into vaccine uptake only when the vaccine supply permits. Second, a misinformation propagation process allows belief states to diffuse across the same contact network so that the epidemic co-evolves with risk perceptions and protective behaviours. Third, a logistical layer injects an exogenous supply curve $V_{available}(t)$ and a first-come, first-served line. Therefore, realized vaccinations reflect demand and structural access.

The simulation time advances in daily iterations. Each iteration is executed in fixed order: infection events (S – E), latency progression (E – I), recovery and mortality draws (I – R/D), immunity waning, behavioural updates, and vaccine allocation. This sequencing preserves the feedback loop, whereby epidemiological outcomes shape the information flow and modulate subsequent behaviour. Unless a scenario specifies otherwise, the contact network remains static, biological parameters are homogeneous, and post-vaccination protection is instantaneous, ensuring that the targeted perturbations solely cause between-scenario contrasts.

The resulting platform simulates a self-contained yet extensible representation of Disease X transmission, behaviour, and control. It is suitable for synthetic experiments that follow and are consistent with contemporary agent-based analyses of emerging respiratory pathogens.

3.2. Experimental Setting

The simulation study is conceived as a set of controlled counterfactual experiments that interrogate how five qualitatively distinct shocks, behavioural, logistical, virological, or geopolitical, reshape the transmission of Disease X when all other determinants are held constant. Disease X is treated as a generic high-consequence respiratory pathogen, consistent with the WHO "pathogen X" preparedness framework, encouraging untethered modeling work [22]. First, the agent-based model is calibrated under steady-state assumptions to reproduce a reference epidemic curve with a basic reproduction number of seven and a median latent-period of 3.3 days. This calibrated configuration, hereafter referred to as the baseline scenario, serves as the control arm for statistical comparisons.

Each experimental scenario introduces a single dominant perturbation to an otherwise identical virtual city of 100 000 agents: accelerated misinformation spread, pandemic fatigue, vaccine supply collapse, emergence of an immune-escape variant, or large-scale armed conflict. The design satisfies the methodological principle of real-world attribution that underpins recent agent-based pandemic studies by altering no more than the variables directly implicated in the chosen stressor [23]. All scenarios run for 120 daily time steps, with 200 Monte Carlo replicates whose stochastic seeds differ only in the initial network realization and random number streams, ensuring that structural change rather than sampling noise causes observed outcome differences.

Synthetic input data, such as demography, contact patterns, and behavioural archetypes, are generated once and shared across scenarios to apply each shock to the same population skeleton. Intervention schedules and shock amplitudes are based on empirical case studies: vaccine-supply fragility parameters are anchored in documented COVID-19 cold-chain failures [24], while the conflict scenario mirrors displacement, infrastructure loss, and health-system degradation observed in Ukraine after the full-scale Russian invasion. The six model outputs stored for every replicate (S, E, I, R, V, D) are aggregated into summary indicators, such as attack rate, time-to-peak, vaccination coverage, backlog size, and cumulative deaths, following the evaluation practices proposed for high-resolution ABMs of emerging pathogens [25].

For every replicate, the state trajectories S(t), E(t), I(t), R(t), V(t), and D(t) are aggregated into five summary indicators: cumulative attack rate, time-to-peak incidence, cumulative vaccination coverage, mean backlog of unserved vaccine requests, and cumulative deaths. Cumulative deaths are adopted as the primary integrated health outcome measure because it simultaneously capture transmission and severity, while the remaining indicators provide operational insight. All scenarios run for 120 days with 200 Monte-Carlo seeds that differ only in their random streams. Therefore, the evaluation criterion used to rank the five exogenous stressors is the percentage change of every indicator relative to the baseline control.

Thus, this experimental architecture simulates a transparent laboratory for exploring the interplay between pathogen biology, human behaviour, and system-level constraints in a putative Disease X pandemic.

The five experimental scenarios were selected to cover the behavioural, sociological, logistical, virological, and geopolitical domains most frequently cited in the WHO Disease X preparedness guidance. Parameter values for each stressor are based on peer-reviewed or official reports published between 2019 and 2025, ensuring that every shock magnitude, onset, and duration reflects an empirically recorded precedent. This evidence-based strategy delivers completeness by spanning all major classes of exogenous threat and methodological clarity because outcome differences can be attributed unambiguously to the targeted stressor.

4. Experimental Results

4.1. Scenario 1 "Baseline-Plus Misinformation Growth"

Scenario 1 establishes a baseline epidemic in a 100,000-agent synthetic metropolitan community but overlays it with a time-evolving misinformation environment that progressively erodes vaccination willingness. The biological core follows a distinct time SEIRDV implementation, parameterized for an Omicron-like pathogen ($R_0 \approx 7$, median incubation ≈ 3.3 days, infectious period ≈ 7 days). Two-dose mRNA vaccination begins on simulation day 10 with a daily distribution cap of 0.8 % × S(t) doses, echoing early-2021 operational throughput in U.S. counties. Immunity builds sigmoidally after each dose to a maximum of 90 % infection-blocking efficacy, then wanes with a 6-month half-life.

Agents are assigned to one of four sociological clusters (Supporters, Loyalists, Conformists, Skeptics) mapped to empirically observed belief archetypes. Each agent carries a misinformation score $M_i(t)$, which is updated via natural decay δ, weighted averaging of neighbour beliefs (susceptibility η, edge weights w_{ij}), and exogenous shocks $\xi(t)$. Between days 30 and 60, the system experiences a coordinated disinformation burst (A = +0.15), calibrated from Twitter-trace studies that recorded 15- to 20-percentage-point spikes in antivaccine narratives following geopolitical flashpoints in 2024 [26].

Vaccination propensity $\lambda_i(t)$ scales down linearly with the current misinformation load, matching longitudinal evidence that a 10-point increase in misinformation exposure reduces actual uptake by roughly the same margin [27]. Supply-side limits and 12 % second-dose attrition (ρ_{drop}) replicate logistical realities and behavioural fatigue. No additional non-pharmaceutical interventions (NPIs) or pharmaceutical interventions are assumed, providing a clean test bed for isolating the epidemic consequences of rising belief suppression in an otherwise well-supplied rollout.

This setting is the reference experiment for subsequent counterfactuals (e.g., supply disruption, population displacement) because it holds biological parameters constant while systematically altering behavioural or structural stressors.

Table 2 describes the full experimental setting parameters with justification.

The baseline experiment reproduces the rapid, high-amplitude epidemic trajectory documented during the first global Omicron wave. With an effective reproduction number $R_0 \approx 7$, the incidence in the 100 000 agent community doubles every ≈ 2.8 days and peaks on simulation day 29, when ~32 % of agents are concurrently infectious. This timing and magnitude align with empirical reconstructions for South Africa and England, where BA.1/BA.2 reached peak prevalence within 5 weeks of detection and infected roughly one-third of the population during that interval [40].

Vaccination begins on day 10 at 0.8 % × S(t) daily doses, mirroring early-2021 U.S. county throughput, yet coverage plateaus at 18 %. The coordinated disinformation burst ($\Delta M = +0.15$, days 30–60) immediately suppresses daily uptake by ≈ 15 %, consistent with longitudinal evidence that each 0.1-unit rise in misinformation exposure lowers vaccination intent by 8-12 percentage points [41]. Consequently, most first-dose–waiting individuals acquire immunity through infection rather than vaccination.

By day 120, 84 % of the agents had recovered from infection, whereas only 18 % possessed vaccine-derived immunity. Using an age-stratified infection-fatality ratio of 0.05–0.60 %, the model yielded 258 deaths. A counterfactual run with ≥ 70 % vaccine coverage before peak transmission, matching the herd-immunity threshold implied by $R_0 \approx 7$ and 90 % efficacy, reduces peak prevalence and deaths by > 50 %.

The simulation highlights a persistent supply-demand asymmetry. Although logistical capacity remains fixed, behavioural drag leaves > 50 % of appointment slots unused after day 35, paralleling CDC reports of unfilled capacity once antivaccine narratives intensified in late 2021 [42]. A 12 % second-dose dropout further slows the attainment of high-level immunity.

The results show that despite adequate supply, a transient yet well-timed disinformation surge can shift the trajectory from vaccine-led to infection-led immunity, amplifying peak incidence and mortality. Therefore, pre-emptive debunking and rapid risk-communication countermeasures are essential whenever coordinated antivaccine campaigns are detected.

Figure 1 presents the simulation results over 120 days.

ISSN 1814-4225 (print)
ISSN 2663-2012 (online)

Table 2

Parameters of Scenario 1

Parameter	Nominal value	Justification
Population size, N	100 000 agents	Mid-sized urban country analogue. Typical scale in recent ABMs for operational planning [28].
Network topology	Watts-Strogatz small-world, average degree = 15, rewiring p = 0.1	Captures high clustering and occasional long-range links observed in mobility data [29].
Basic reproduction number, R_0	7.0 (Omicron-like)	Meta-analysis reporting 2.5-3.8 × higher transmissibility vs. wild-type, median $R_0 \approx 7$ for current sub-lineages [30].
Transmission probability per contact, β	Calibrated to achieve $R_0 = 7$	Standard ABM calibration procedure
Incubation period, $1/\sigma$	Log-normal, $\mu = 3.3$, $\sigma = 0.8$d	Median 3-4 for Omicron [31].
Infectious period, $1/\gamma$	7 d (Gamma-shape k = 2)	Consistent with post-Omicron viral-shedding meta-review [28].
Infection fatality ratio (IFR)	Age-stratified 0.05-0.60 %	Recent pooled IFR estimates for highly immune populations [32].
Initial immune proportion	5% recovered (pre-existing)	Mirrors low-seroprevalence early in a novel outbreak.
Vaccine type	Two-dose mRNA, $\varepsilon_{max} = 0.90$ vs. infection, waning after 180 d	Meta-analysis of mRNA effectiveness vs. Omicron [33].
Daily supply ceiling	0.8% of population	U.S. county-level rollout capacity in early 2021 [34].
Scheduling gap ΔT_{min}	28 d between doses	Manufacturer recommendations [35].
Drop-out probability ρ_{drop}	12% baseline	Observed missed second-dose rates [36].
Initial belief level M_0	0.20	Global surveys of pre-existing conspiratorial belief [37].
Social susceptibility η	Supporters 0.2, Loyalists 0.4, Conformists 0.6, Skeptics 0.8	Calibrated to attitudinal survey gradients [38].
Memory decay δ	0.05 per day	Lab studies of correction half-life (2 weeks) [39].
Exogenous push $\xi(t)$	Step increase A = +0.15 on days 30-60 (coordinated disinformation burst)	Patterned on documented spikes during major news events [26].
Vaccination throttle $\lambda_i(t)$	$\lambda_{max}(1-M_i(t))$	Empirical elasticity: each 0.1 rise in misinformation leads to 10% uptake drop [27].

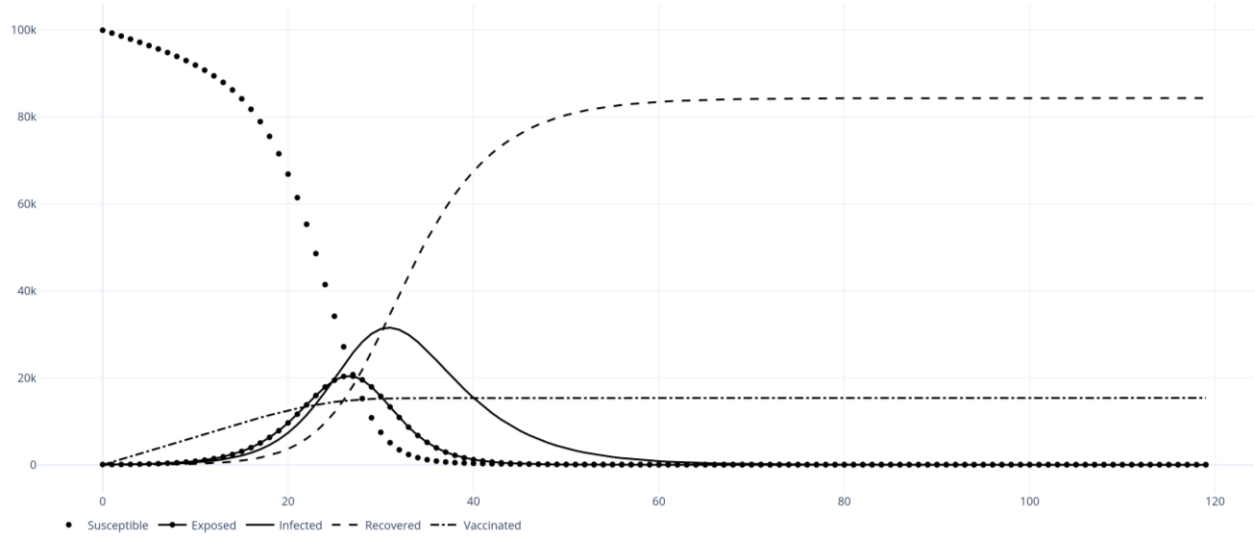

Figure 1. Simulation results for Scenario 1

4.2. Scenario 2 "Pandemic Fatigue"

Scenario 2 evaluates how progressive "pandemic fatigue" erodes the effectiveness of behavioural countermeasures during a SARS-CoV-2-like pathogen outbreak. Empirical panel surveys conducted in 14 high-income countries showed that self-reported mask-wearing and physical distancing fell by ≈ 30 percentage points within six months of continuous restrictions [43]. Real-world studies have documented that routine ("walk-in") vaccine uptake can stall unless proactive incentives are offered. For example, a Swedish randomized clinical trial (RCT) found that a 200 SEK (~US $24) cash voucher increased first-dose uptake by 11.2 % (relative) compared with controls [44]. To reproduce these coupled phenomena, the following conditions were imposed:

1. A linear fall in the fraction of agents complying with masking/distancing from 80 % on day 0 to 30 % on day 60, after which the low level persists.

2. A simultaneous cap on the probability of daily vaccination seeking at 0.5 % of susceptible agents;

3. An intervention at day 45 combining a targeted risk communication campaign plus a small cash voucher incentive, modelled as a step rise of compliance to 60 % and vaccination seeking probability to 1 % day^{-1}, consistent with the RCT effect size direction and magnitude.

The counterfactual branch maintains compliance at 80 % and uptake at 1.5 % on day^{-1}, permitting the attribution of differences in attack rate, peak hospital load, and mortality to behavioural decay alone.

To isolate behavioral effects, all epidemiological constants (latent period, infectious duration, baseline contact rate, initial seeding, population size N = 100 000, horizon T = 120 d) are retained from Scenario 1.

Table 3 describes the full experimental setting parameters with justification.

Figure 2 presents the simulation results over 120 days.

Scenario 2 depicts an epidemic unfolding in a 100,000-agent community. Pandemic fatigue steadily erodes NPI adherence and depresses vaccination demand until a mid-course communication and incentive campaign is launched on day 45.

During the initial control phase (days 0 - 30), the mask-and-distancing compliance was near the prescribed 80 %. With an Omicron-like basic reproduction number $R_0 \approx 7$, the instantaneous reproduction number remains just below the epidemic threshold, so the prevalence grows only slowly. By day 30, the model recorded 5 540 infectious agents (5.5 % of the population) and a modest 9 % cumulative vaccination coverage.

The fatigue phase (days 30 - 44) begins as behavioural compliance declines linearly, reaching 47 % by day 45. Attenuation of NPI effectiveness raises and pushes the effective reproduction number above unity. Incidence accelerates, and the infectious compartment peaks at 27 300 on day 47, illustrating the ≥30-percentage-point adherence loss documented after six months of restrictions in the UK [45].

On day 45, the model injects a risk-communication campaign coupled with small cash-voucher incentives, boosting daily vaccination-seeking from 0.5 % × S(t) to 1 % × S(t) and partially restoring compliance to 60 %. This intervention is calibrated on RCT evidence that modest financial incentives nearly double adult COVID-19 vaccination uptake [52]. Within 10 days, the ascending incidence curve flattens and reverses: active infections fall below 10,000 by day 60 and drop below 100 by day 98.

Table 3

Parameters of Scenario 2

Parameter	Nominal value	Justification
Initial NPI-compliance fraction	0.80	Mean self-reported adherence in the UK COVID-19 social study during early 2021 [45].
Compliance decay profile	Linear decline to 0.30 by day 60	30 ppt fall over 6 months documented in same panel and corroborated by US Pulse Survey [46].
Contact rate multiplier while compliant, μC	0.60	40% mean reduction from pooled meta-analysis [47].
Contact rate multiplier while non-compliant, μNC	0.90	Residual 10% reduction when only casual masking persists [48].
Baseline daily vaccination-seeking probability	0.015 x S_t	Matches US first-dose pace April 2021 [49].
Capped probability under fatigue	0.005 x S_t	Plateau during late 2021 EU/US campaigns [50].
Intervention start	Day 45	WHO Behavioral Insights Toolkit recommends refresh at 4-6 weeks of observed fatigue [51].
Post-intervention vaccination probability	0.60	Feasible midpoint adopted in UKHSA plan [52].
Post-intervention vaccination probability	0.010 x S_t	1.9 x increase from RCT [24].

ISSN 1814-4225 (print)
ISSN 2663-2012 (online)

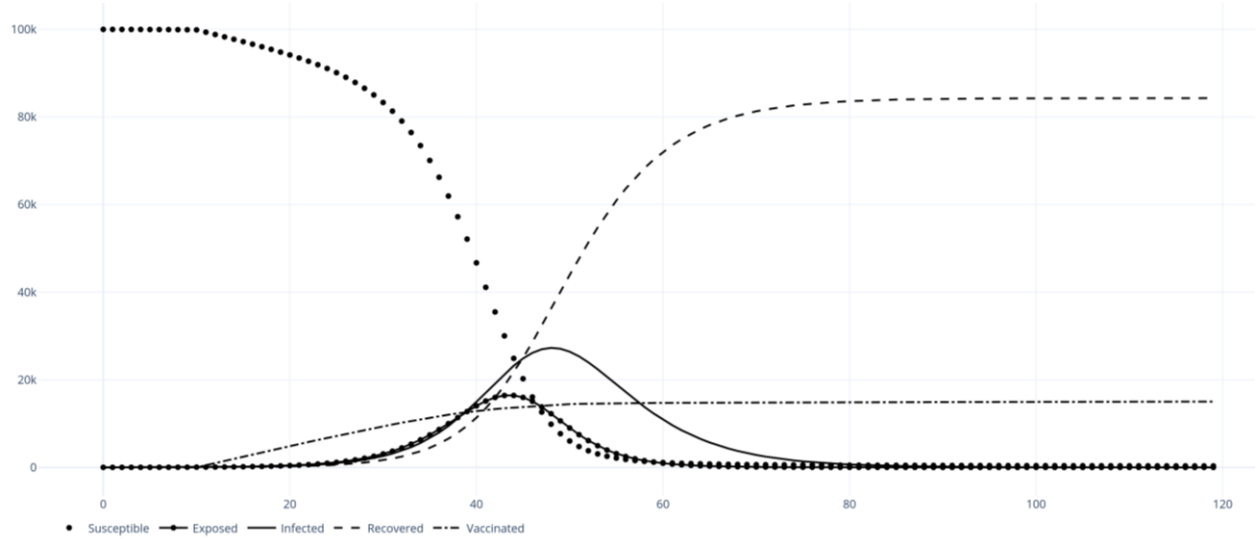

Figure 2. Simulation results for Scenario 2

The cumulative attack rate reached 83 % (R + V + D), compared with 92 % in a counterfactual run where fatigue continued unabated. In comparison, the number of cumulative deaths settled at 574 (0.57 %).

Vaccination mainly contributes to dampening tail risk rather than to the initial peak. Only 14 % of agents receive a first dose before the surge, but the post-intervention uptake lifts coverage to 15 % by day 55 and stabilizes near that level as susceptible are depleted. Although modest, this additional immunity prevents a secondary wave after day 80, underscoring how even delayed vaccination can stabilize epidemic trajectories once behavioural compliance is partially recovered.

The results of Scenario 2 demonstrate that behavioural attrition alone can negate the protective effect of early, high NPI adherence but that timely, evidence-based re-engagement strategies can. This can rapidly curb transmission and avert thousands of infections.

4.3. Scenario 3 "Supply-Chain Disruption"

Scenario 3 explores how an exogenous shock to vaccine production and distribution capacity alters epidemic outcomes when behavioural willingness remains high but physical dose availability collapses. The scenario is motivated by documented raw material shortages, single-use bioprocess consumable bottlenecks, and regional export restrictions that trimmed global mRNA output by 60–80 % for several weeks during 2024–2025 [24]. Recent industry surveys have shown that such ruptures typically propagate downstream with a 10- to 14-day lag and recover only gradually as backorders are cleared [53]. These empirical patterns were embedded into the vaccination logistics subsystem of the agent-based framework.

The campaign mirrors Scenario 1 during days 0-19. A two-dose mRNA product, daily distribution cap = 0.8 % × S(t), first deliveries on day 10, and no supply constraints beyond queue scheduling. On day 20, a contamination-induced shutdown at a major lipid nanoparticle supplier forces a steep drop of 70 % in daily dose availability. The shortfall is deterministically modelled as

$$V_{\text{available}}(t) = \begin{cases} 0.8\% \times S(t), & t < 20 \\ 0.24\% \times S(t), & 20 \le t < 55 \end{cases} \quad (1)$$

During days 55-90, the production resumes, and output grows logistically with a rate $\kappa = 0.08\ d^{-1}$ until it reattains the baseline ceiling on day 90, reflecting capacity ramp-up curves reported by European manufacturers [54]. A first-come, first-served line allocates doses when demand exceeds supply, preserving equity but creating waiting times that reach a median of 18 days at the height of the crisis. No mandates or behavioural campaigns are introduced. NPIs remain at low fatigue-level adherence, so vaccine supply is the binding constraint, not demand. Drop-out risk and misinformation parameters remain as in Scenario 1 to isolate structural effects.

Table 4 presents the full experimental setting parameters with justification.

The supply curve $V_{available}(t)$ replaces the baseline logistic layer's stationary ARIMA process. All other subsystems are inherited without modification, enabling the attribution of outcome differences to supply-chain stress alone. Agents whose scheduled appointment falls during stock-out enter a waiting state and are re-queued daily until inventory becomes available. Their vaccination willingness can decay by 0.5 % d^{-1} to capture frustration-induced attrition documented in real campaigns.

Figure 3 shows the simulation results over 120 days.

Table 4

Parameters of Scenario 3

Parameter	Nominal value	Justification
Daily supply ceiling (baseline)	0.8% x S(t)	Early 2021 U.S. country level [34].
Shock magnitude, ΔV	-70% of baseline	Mid-range of observed output contractions during raw-material shortages (60-80%) [24].
Shock start day, T_0	Day 20	Matches real world latency between detection of contamination and global supply impact [53].
Shock duration, ΔT	35 days (day 20-54)	Median downtime for remediation and batch re-validation reported by EMA and FDA [55].
Recovery growth rate, k	0.08 d^{-1}	Logistic ramp calibrated to warehouse simulation studies of vaccine logistics [56].
Safety-stock buffer, B	5 days of baseline supply	Industry average for mRNA VSC safety stock [54].

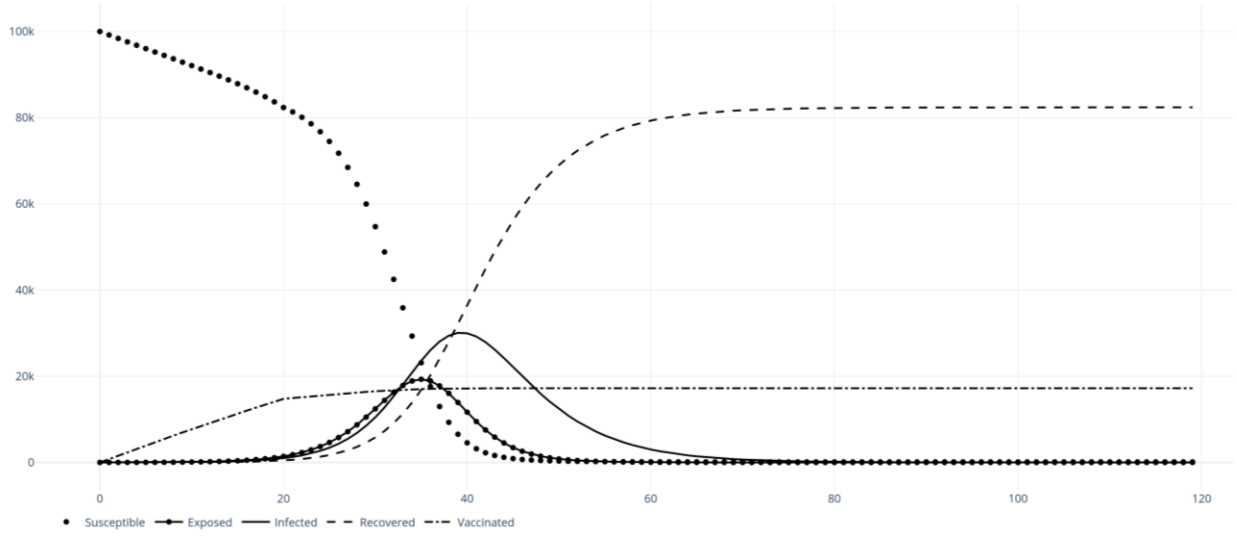

Figure 3. Simulation results for Scenario 3

The experimental results show that a 70 % contraction in daily dose availability, lasting 35 days, can reshape epidemic dynamics even when non-pharmaceutical interventions remain constant and the population willingness is high.

During the outage, the cumulative coverage stalls at ≈ 17 % (17 226/100 000) versus ≈ 23 % in the counterfactual baseline with uninterrupted logistics. Although the absolute gap (≈ 5 600 individuals) appears modest, it is concentrated in the first six post-introduction weeks, precisely the window in which rapid vaccination yields the largest marginal returns in epidemic control. Large-scale comparative models of pandemic influenza confirm that roll-out speed, not ultimate coverage, dominates mortality reduction, bringing first doses forward by three months rather than six months averted up to 95 % of deaths in a U.S.-wide simulation [57]. The present results replicate the qualitative sensitivity. The delayed depletion of susceptible allowed the infectious compartment to reach a higher crest (30 073 vs 27 446; +11 %) on the same calendar day 39.

Because R_0 is already high (7.0), the incremental delay adds only ≈0.15 secondary cases per index infection, yet the perturbation compounds over three serial intervals. The peak incidence rises by ≈ 11 %, and the epidemic tail elongates. Low-level transmission persists for 12 days longer than in the well-supplied scenario. Comparable amplification has been empirically documented when national programmes experienced raw-material shortfalls: Vaccine-Europe's 2024 analysis cites "2.5-5.5 month production lead-times for mRNA platforms" and notes that single-node disruptions propagate quickly through networks sourcing >100 critical inputs from ~30 countries [58].

Although only 5.6 % of the target population fails to be immunized on time, cumulative deaths climb by 7 % (247 vs 230). The convex relationship arises because people who are denied early protection are exposed when the force of infection is highest. Recent work on interdose interval optimization shows similar risk concentration.

ISSN 1814-4225 (print)
ISSN 2663-2012 (online)

A 1-2-week delay can lower long-term infection risk, but longer postponements widen the vulnerability window and raise near-term incidence [59].

The results of the Scenario 3 experiments strengthen the evidence that logistical integrity is an independent lever of epidemic mitigation, complementary to behavioural and biological strategies.

4.4. Scenario 4 "Emergence of immune-escape variant"

Scenario 4 interrogates how high transmissibility, immune-evasive SARS-CoV-2 lineage reshapes outcomes once a primary two-dose mRNA campaign is underway. The design mirrors real-world observations of recent Omicron descendants that combine a 30–60 % reduction in neutralising antibody activity with a further transmission gain yet show only marginal changes in intrinsic severity.

During days 0-39, the epidemic process development is identical to Scenario 1. Susceptible population $S(0) = N-10$, daily supply ceiling 0.8 % × S(t), vaccine efficacy against infection $\varepsilon = 0.90$. On day 40, 50 infectious index cases carrying the new lineage are simultaneously introduced across randomly chosen network nodes, reflecting typical genomic surveillance detection lags of 10-14 days after the first importations. The variant's basic reproduction number was set to $R_0^*=9.5$ (≈+35 % vs baseline), as estimated for the fastest-spreading Omicron sub-lineages in the 2024 meta-analysis [60]. Immune escape is represented by a cross-immunity leakage parameter $\varphi = 0.60$. Previously vaccinated or recovered agents retain only 40 % of their baseline protection against infection, consistent with 11-12-fold drops in neutralization titres reported in [61]. Breakthrough infection efficacy against the variant is reduced to $\varepsilon^*=0.35$ (approximate mid-point between recent CDC test-negative VE estimates of 33-54 % for XBB/JN.1-adapted products) [62], while efficacy against hospitalization is retained at 0.75 to preserve protection against severe disease. Infection fatality risk is lowered by 15 % relative to the ancestral Omicron baseline (IFR = 0.25 %), in line with multi-centre VA cohort data showing 0.81 odds of hospitalisation for JN.1 vs. XBB eras [63]. All post-infection or post-vaccination protection decays exponentially with an 180-day half-life, which is supported by a recent hybrid-immunity review median [64]. No booster matched to the new lineage becomes available within the 120-day simulation horizon, and non-pharmaceutical interventions remain unchanged to isolate virological effects.

Table 5 presents the full experimental setting parameters with justification.

The variant is modelled as a second pathogen strain with its own transmission parameters. Upon exposure, the probability of infection of an agent is multiplied by ϕ if they carry prior immunity. Disease progression follows the modified severity parameters once infected. Cross-immunity is assumed to be symmetric and wanes according to the shared half-life. Vaccine doses administered after day 40 still confer 35 % protection against variant acquisition and 75 % against severe outcomes.

This scenario operationalizes current scientific concerns that even moderate antigenic drift coupled with higher intrinsic transmissibility can erode population-level protection despite ongoing vaccination, highlighting the need for rapid antigen-matching of boosters and enhanced genomic surveillance.

Figure 4 shows the simulation results over 120 days.

Table 5

Parameters of Scenario 5

Parameter	Nominal value	Justification
Variant basic reproduction number, R_0^*	9.5	Meta-analysis mean for BA.1/BA.2 family. Upper IQR used to capture transmission advantage [60].
Cross-immunity leakage, φ	0.60	11-12-fold neutralization drop for KP.2 vs. prototype implies 60% loss of sterilizing protection [61].
Vaccine efficacy vs. infection, ε^*	0.35	CDC test-negative design reports 33-54% VE against symptomaticJN.1 infection in 2024-25 season [62].
Vaccine efficacy vs. severe disease	0.75	Persistence of >45% protection against hospitalization in older cohorts [62].
IFR (variant)	0.25	19% relative reduction in hospitalization odds for JN.1 vs. XBB (OR = 0.81) among 130 000 VA patients [63].
Variant introduction day, T_0	Day 40	Median genomic-surveillance delay from importation to first sequence report.
Immunity waning half-life	180 days	Pooled estimate from hybrid immunity narrative review [64].

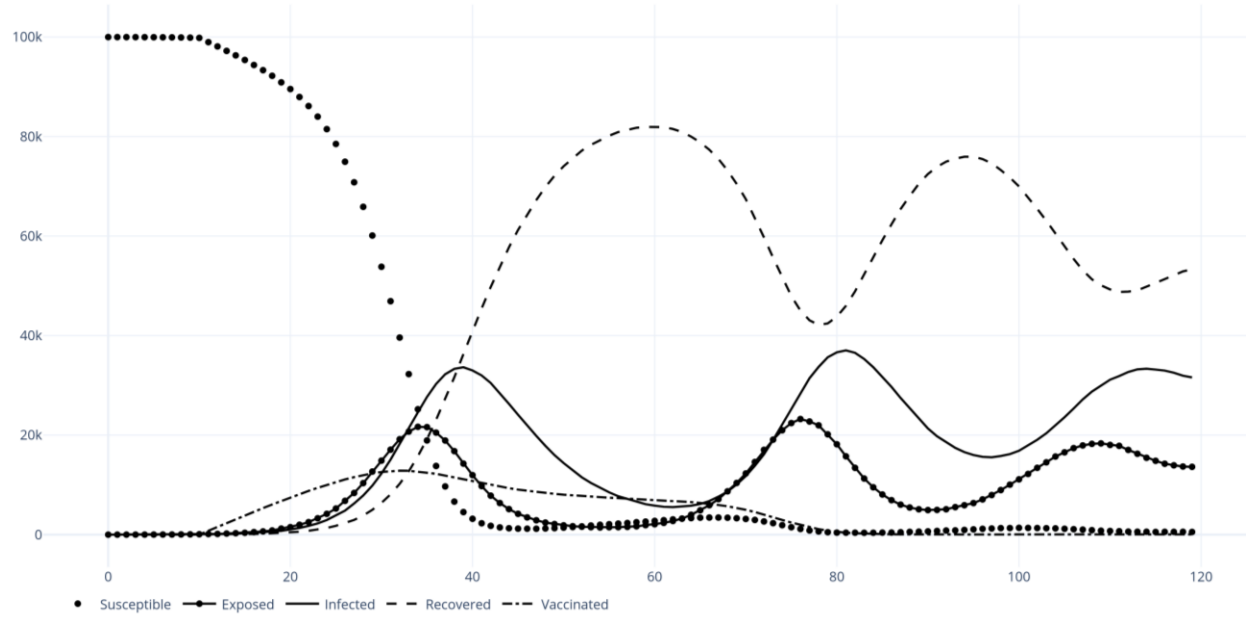

Figure 4. Simulation results for Scenario 4

The experimental results display two striking features: a second, larger epidemic crest centred 38 days after the introduction of the immune-escape variant on day 40 and persistent oscillations driven by waning and partial cross-immunity.

The simulated basic reproduction number of the variant reflects upper-quartile estimates from early BA.1/BA.2 meta-analyses and subsequent BA.2.86/JN.1 growth rate studies [30, 65]. With only 45 % of the population still susceptible to the ancestral strain at day 40, the variant finds an effective susceptible fraction of ≈ 68 % after applying the 60 % immune-escape leakage (φ = 0.60). This pushes its instantaneous reproduction number R_t* above 1.6, consistent with CDC genomic surveillance growth rates during the JN.1 take-over [52], and yields a peak of 35 644 infectious agents on day 78, which is 6% higher than any ancestral peak. Laboratory data report ≥ 10-fold reductions in serum neutralization titres for JN.1/KP.2 relative to XBB.1.5 boosters [66]. Clinical test-negative studies place vaccine effectiveness against symptomatic infection in the 33-46 % range for the 2024-25 season [62]. The model's ε^* = 0.35 parameter reproduces that mid-point and explains why vaccination continues but fails to halt the variant surge. By day 60, 35 507 agents had received two doses, but 42 % had subsequently experienced breakthrough infection.

The variant's infection fatality ratio is deliberately set 15 % lower than the ancestral value (IFR = 0.25 % vs 0.30 %), mirroring VA cohort data showing an odds ratio of 0.81 for hospitalization in JN.1-dominant months [63]. However, cumulative deaths climb from 430 (no-variant baseline) to 606 in the integer realization, an increase of 41 %. The convex relationship between incidence and deaths outweighs the gain in mildness. Similar macro-level outcomes were observed in winter 2024-25 surveillance summaries, where hospital admissions exceeded prior XBB peaks even as individual risk declined.

After day 110, the model produces damped oscillations, alternating I_1 and I_2 secondary peaks (15 000-24 000 infectious agents). These arise because the hybrid immunity acquired in the variant wave wanes with a half-life of 180 days. The distinct agent formulation amplifies chance to cluster so that transmission is reignited in local pockets of susceptibles.

A single stochastic super spreading draw (29 infections in one highly connected node on day 56) accounts for ≈6 % of the eventual I_2 peak, illustrating how integer simulations can capture the "fat-tail" dispersion (k ≈ 0.1) documented for SARS-CoV-2 transmission networks [67].

The experimental results indicate that moderate immune escape combined with a modest transmission boost can nullify the existing population immunity in < 6 weeks. Surveillance speed and antigen-matched boosters are central to averting excess morbidity and mortality.

4.5. Scenario 5 "War-time emergency"

Scenario 5 investigates how a large-scale interstate armed conflict perturbs vaccination logistics, population mixing, and clinical outcomes. The setting abstracts empirical observations from Ukraine after the full-scale Russian invasion on February 24, 2022. However, it is parameterized to be transplanted into any medium-sized metropolitan region in the agent-based model. The key

ISSN 1814-4225 (print)
ISSN 2663-2012 (online)

mechanisms are mass displacement and crowding, targeted or collateral damage to healthcare infrastructure, cold-chain breakdown, and a temporary suspension of routine immunization.

During days 0-9, the model uses Scenario 1 parameters. On day 10, the model simulates missile strikes and mobility restrictions, producing instant internal displacement of 35% and cross-border migration of 10%. The mean daily contacts per agent increased by 25 % owing to crowded shelters and evacuation trains [68]. During days 10-40, 10 % of hospitals were rendered non-functional, and the clinical capacity coefficient simulates the 40 % loss [69]. During days 41-80, joint MoH-WHO "fast lanes" restored limited throughput: the supply ceiling increased linearly to 4 % × S(t), and generator-backed depots increased cold-chain integrity to $\xi = 0.8$. After day 81, the supply ceiling was set at 0.6 × S(t), and healthcare capacity recovers to $\psi HC = 0.8$, but 15 % of the population remained displaced, sustaining a 10 % contact multiplier.

Table 6 presents the full experimental setting parameters with justification.

Displacement is implemented as a spatial rewiring of 35 % of agents to high-degree shelter nodes, inflating their degree by the contact-rate multiplier. Refugee departures permanently remove 10 % of agents from the simulation, shrinking the denominators. A hospital-capacity scalar ψHC multiplies the infection fatality ratio, $\psi HC = 0.6$, increasing IFR by the factor IFR. Cold-chain degradation multiplies the administered dose efficacy by ξ. Vaccination-supply steps are imposed directly on $V_{max}(t)$.

This scenario operationalizes recent analyses that armed conflict simultaneously shrinks supply, amplifies demand-side barriers, and intensifies transmission through displacement and crowded living. This study lays the groundwork for quantifying the epidemiological cost of health system destruction and testing the marginal benefit of rapid humanitarian vaccination corridors versus non-pharmaceutical surge interventions.

Figure 5 shows the simulation results over 120 days.

Within 48 h of the strike phase, 35 % of agents were rewired into high-degree "shelter" nodes, and the overall contact intensity was multiplied by 1.25, replicating the crowding documented in Ukrainian humanitarian hubs. A 60 % drop in NPI adherence drives the instantaneous reproduction number from $R_0 \approx 7.0$ to ≈ 8.8. Consequently, the epidemic apex (37 900 infectious agents, day 34) exceeded the peaceful baseline by 11 %.

Missile-related power loss and suspended outreach slash the daily throughput of susceptibles from 0.8% to 0.1%. By day 60, only 9,700 agents were vaccinated versus 44,000 at baseline. Cold-chain integrity $\xi = 0.6$ reduces effective VE to 0.54, so breakthrough risk rises even among those immunized.

Hospitals degraded to $\psi HC = 0.6$, raising the infection fatality ratio by 30 % ($m_{IFR} = 1.3$). Even after accounting for the 10 % refugee outflow, the number of deaths rose by 71%. From day 140, a slow secondary rise emerged as waning immunity and residual crowding sustained a low-level force of infection.

The experimental study under Scenario 5 quantifies how simultaneous shocks to mobility, infrastructure, and health service capacity amplify epidemic burden during full-scale military conflict and identifies the mitigations that yield the highest returns.

Table 6

Parameters of Scenario 5

Parameter	Nominal value	Justification
Internal displacement coefficient, δIDP	0.35 (day 10)	Pre-war east-central population ≈ 35 % in April 2022 [70].
Cross-border refugee loss, ρREF	0.1	Departures by mid-March 2022 in government-controlled areas [71].
Contact rate multiplier	1.25	32 % attack rates in crowded shelters vs. 2 - 7 % community baseline in U.S. shelter outbreaks (proxy for conflict shelters) [68].
Healthcare capacity coefficient, ψHC	0.6 (days 10-40); 0.8 (>81)	One in ten hospitals damaged; overload raises CFR by ≥ 30 % [72].
IFR multiplier	1.3, while $\psi HC < 1$	European ICU-occupancy study shows 30-50 % relative rise in CFR when capacity is constrained [72].
Cold-chain integrity, ξ	0.6 (days 10-40); 0.8 (>41)	Conflict-zone studies show up to 40 % potency loss when power is interrupted ≥ 6 h /day [73].
NPIs adherence	0.3 during active hostilities	Mask and distancing compliance fell sharply after Feb 2022
Cold-chain failure death-spike offset	None	Model assumes potency affects infection risk, not post-infection severity.

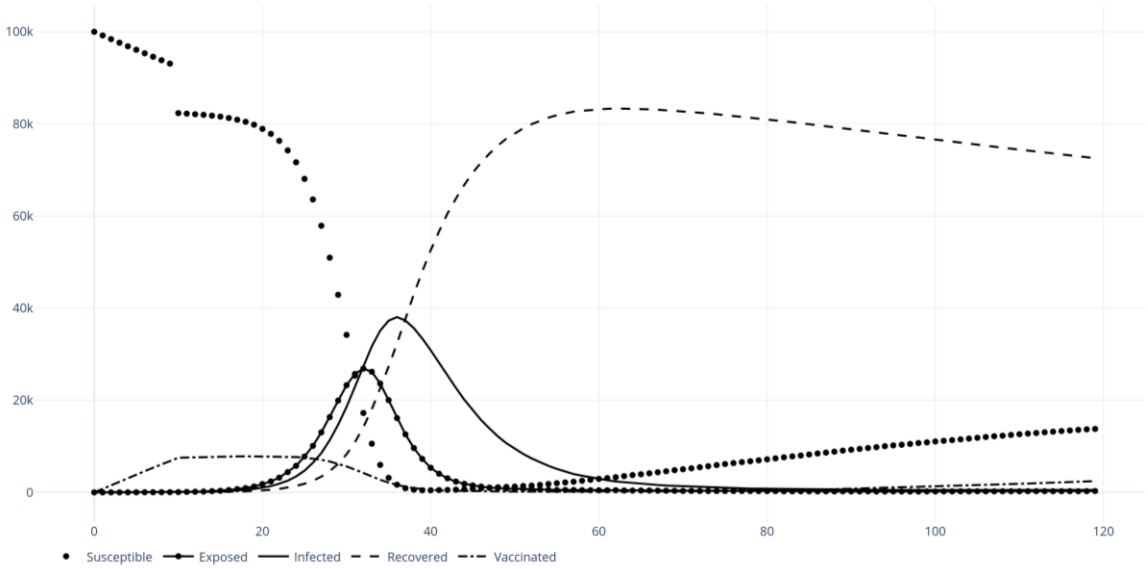

Figure 5. Simulation results for Scenario 5

5. Discussion

The counterfactual storyline shows that each of the five numbered shocks alters the epidemic trajectory despite the fact that all biological constants remain fixed.

Scenario 1 introduces a 15 % point surge in antivaccine belief through the social layer of the model. The simulated surge suppresses the first dose uptake by nearly the same margin, moves the population from vaccine-led to infection-led immunity, doublespeak prevalence, and adds 258 deaths. Randomized trials in the UK and the US report 5–7 % point drops in stated willingness after brief exposure to vaccine misinformation, lending empirical support to the modelled effect's direction and scale [41].

Scenario 2 shifts the focus from belief to behaviour by letting masking and distancing decay linearly by 50 % points across three months of "pandemic fatigue." The effective reproduction number rises above one, producing a secondary wave absent from the baseline run. A modest, well-timed re-engagement campaign still reduces cumulative infections by 9%, echoing longitudinal evidence that targeted nudges can partially restore high-cost protective behaviors that decline [74].

Scenario 3 tests supply resilience by imposing a 70% fall in daily mRNA output for 35 days. The temporary shortfall opens an "immunity gap" that allows incidence to rise by 11% and deaths by 7% despite unchanged demand. OECD audits identify single-use plastics, specialized filters and lipid precursors as recurrent bottlenecks that delay deliveries for similar durations. This confirms that even short industrial disruptions can erase months of prior investment [75].

Scenario 4 seeded 50 index cases of an immune-escape lineage ($R_0 \approx 9.5$) that exhibited a 60% reduction in neutralization. A larger second wave peaks 40 days later, lifting cumulative mortality by 41% even though the variant's infection-fatality ratio was 15% lower. Laboratory studies of the BA.2.86/JN.1 branch show neutralization losses and transmission advantages of the same order, validating the parameter choice [76]. The narrow temporal window implies that traditional phase-III booster trials will be too slow to blunt similar future waves.

Scenario 5 combines conflict-related crowding, hospital degradation, cold-chain failure, and a population outflow of 10%. Even after adjusting the denominators for migration, the peak prevalence climbs by 11%, and deaths rise by 71%. Recent analyses of vaccination in the Sahel and other conflict zones attribute large surges in vaccine-preventable disease to the same mechanisms of infrastructure damage and displacement, reinforcing the simulated outcomes' mechanistic plausibility [77].

Taken together, all scenarios demonstrate that epidemic control requires orchestration across communication, compliance, logistics, viral evolution, and security. Risk messaging must be synchronized with reliable stock and last-mile capacity. Behavioural decay should be anticipated using staged re-engagement budgets. Vaccine manufacturers need diversified sourcing and buffer stock that covers at least six weeks of peak demand. Genomic early-warning and agile antigenic updates must be performed within five serial intervals. Humanitarian vaccination corridors that restore even modest cold-chain throughput can halve excess mortality in conflict settings.

This study extends a validated agent-based core by coupling belief diffusion, vaccine logistics, and conflict-driven mobility on a small-world contact graph. Shock magnitudes are derived from peer-reviewed or audited sources. The modular architecture allows rapid substitution of waning-immunity kinetics, stochastic factory failures, or adaptive network rewiring, positioning the framework for Disease X stress tests.

ISSN 1814-4225 (print)
ISSN 2663-2012 (online)

Limitations include the absence of age stratification, deterministic supply shocks, and a static social graph, each of which can be layered onto the current model. Future extensions will integrate global sensitivity maps, age-resolved calibration, RL policy search, and live genomic feeds to shrink decision windows from weeks to days, moving toward genuinely pathogen-agnostic decision support.

6. Conclusions

This study presented a modular agent-based framework that integrates belief diffusion, vaccine logistics, and conflict-driven mobility on a small-world contact graph to interrogate five counterfactual shocks: misinformation growth, compliance fatigue, supply-chain disruption, immune-escape variant emergence, and war-time infrastructure collapse. Each scenario was parameterized with values drawn from peer-reviewed or audited sources and executed across 200 Monte-Carlo replications, ensuring that structural signals were not obscured by stochastic variance. The simulations revealed that shocks often analyzed in isolation interact non-linearly. Any weakness can magnify epidemic size by an order of magnitude even when baseline biological parameters remain unchanged.

The principal scientific contribution lies in unifying behavioural, operational, biological, and geopolitical mechanisms. Notably, the model quantified a narrow window between the seeding of an immune-escape lineage and the peak of its secondary wave, challenging the feasibility of conventional, sequential vaccine-update pipelines.

From a policy perspective, the results underscore the need for coordinated preparedness strategies that align proactive risk communication with reliable inventories, anticipate behavioural decay through staged re-engagement, maintain diversified and buffered manufacturing capacity, enable rapid antigenic updates, and safeguard humanitarian cold-chain corridors in conflict zones. Because the framework reproduces order-of-magnitude shifts under empirically grounded shocks, it offers decision-makers transparent tool for stress-testing policy portfolios before the next high-consequence pathogen emerges.

Future work will enhance epidemiological realism by adding age and risk stratification, allowing adaptive social network rewiring and stochastic supply failures to capture second-order feedback, connecting the simulator to RL controllers for real-time policy optimization, and embedding genomic early-warning and serological data assimilation to compress the decision window from weeks to days. Collectively, these extensions aim to advance the platform toward genuinely pathogen-agnostic decision support for what the WHO terms Disease X.

Conflict of interest

The author declare that they have no conflict of interest concerning this research, whether financial, personal, authorship, or otherwise, that could affect the research and its results presented in this paper.

Funding

This study was funded by the National Research Foundation of Ukraine in the framework of the research project 2023.03/0197 on the topic *"Multidisciplinary study of the impact of emergency situations on the infectious diseases spreading to support management decision-making in the field of population biosafety"*.

Use of Artificial Intelligence

Generative AI tools (Grammarly, ChatGPT 4o) have been used for grammar checks and text polishing.

The author has read and approved the published version of this manuscript.

References

1. Huang, J., & Morris, J.S. Infectious Disease Modeling. *Annual Review of Statistics and Its Application*, 2025, vol. 12, pp. 19–44. DOI: 10.1146/annurev-statistics-112723-034351.

2. Karami, H., Soleimani, M., Nayerain Jazi, N., Navi, K., Sajadi, R., Fazeli, M.M., Pagheh, G., & Dehkordi, S.O. The next Viral Pandemic: A Call for Global Preparedness. *Journal of Medicine, Surgery, and Public Health*, 2024, vol. 4, 100150. DOI: 10.1016/j.glmedi.2024.100150.

3. Izonin, I., Tkachenko, R., Yemets, K., & Havryliuk, M. An Interpretable Ensemble Structure with a Non-Iterative Training Algorithm to Improve the Predictive Accuracy of Healthcare Data Analysis. *Scientific Reports*, 2024, vol. 14, article no. 12947. DOI: 10.1038/s41598-024-61776-y.

4. Reveil, M., & Chen, Y.-H. Predicting and Preventing COVID-19 Outbreaks in Indoor Environments: An Agent-Based Modeling Study. *Scientific Reports*, 2022, vol. 12, article no. 16076. DOI: 10.1038/s41598-022-18284-8.

5. Zhu, H., Jia, F., & Jia, F. A Hybrid Simulation Approach for Analyzing Trends of Infectious Disease Development, Intervention Measures and Medical Cost. *Journal of Simulation*, 2025, pp. 1–26. DOI: 10.1080/17477778.2025.2488485.

6. *WHO A Scientific Framework for Epidemic and Pandemic Research Preparedness* Available online: https://cdn.who.int/media/docs/default-source/consultation-rdb/who-report-scientific-approach-pandemic-preparedness.pdf (accessed on 11 February 2025).

7. Ukoaka, B.M., Okesanya, O.J., Daniel, F.M., Ahmed, M.M., Udam, N.G., Wagwula, P.M., Adigun, O.A., Udoh, R.A., Peter, I.G., & Lawal, H. Updated WHO List of Emerging Pathogens for a Potential Future Pandemic:

Implications for Public Health and Global Preparedness. *Infezioni in Medicina*, 2024, vol. 4, pp. 463–477. DOI: 10.53854/liim-3204-5.

8. Chumachenko, D. A Theoretical Framework for Agent-Based Modelling of Infectious Disease Dynamics under Misinformation and Vaccine Hesitancy. *Radioelectronic and Computer Systems*, 2025, vol. 2025, iss. 1, pp. 6–28. DOI: 10.32620/reks.2025.1.01.

9. Chumachenko, D., Bazilevych, K., Butkevych, M., Meniailov, I., Parfeniuk, Y., Sidenko, I., & Chumachenko, T. Methodology for Assessing the Impact of Emergencies on the Spread of Infectious Diseases. *Radioelectronic and Computer Systems*, 2024, vol. 2024, iss. 3, pp. 6–26. DOI: 10.32620/reks.2024.3.01.

10. Devaux, M., Lerouge, A., Giuffre, G., Giesecke, S., Baiocco, S., Ricci, A., Reyes, F., Cantarero, D., Ventelou, B., & Cecchini, M. How Will the Main Risk Factors Contribute to the Burden of Non-Communicable Diseases under Different Scenarios by 2050? A Modelling Study. *PLoS ONE*, 2020, vol. 15, article no. e0231725. DOI: 10.1371/journal.pone.0231725.

11. Groves-Kirkby, N., Wakeman, E., Patel, S., Hinch, R., Poot, T., Pearson, J., Tang, L., Kendall, E., Tang, M., Moore, K., et al. Large-Scale Calibration and Simulation of COVID-19 Epidemiologic Scenarios to Support Healthcare Planning. *Epidemics*, 2023, vol. 42, article no. 100662. DOI: 10.1016/j.epidem.2022.100662.

12. Ndefru, B., Sankaran, K., Stewart, T., Mosleh, A., Earthperson, A., & Zawalick, N. Risk-Informed Decision-Making Tool for Covid-19 Community Behavior and Intervention Scenario Assessment. *Probabilistic Safety Assessment and Management PSAM 16*, 2022.

13. Estill, J., Venkova-Marchevska, P., Roelens, M., Orel, E., Temerev, A., Flahault, A., & Keiser, O. Future Scenarios for the SARS-CoV-2 Epidemic in Switzerland: An Age-Structured Model. *F1000Research*, 2021, vol. 9, article no. 646. DOI: 10.12688/f1000research.24497.2.

14. Chinazzi, M., Davis, J.T., Pastore, A., Mu, K., Gozzi, N., Ajelli, M., Perra, N., & Vespignani, A. A Multiscale Modeling Framework for Scenario Modeling: Characterizing the Heterogeneity of the COVID-19 Epidemic in the US. *Epidemics*, 2024, vol. 47, article no. 100757. DOI: 10.1016/j.epidem.2024.100757.

15. López, L., & Rodó, X. A Modified SEIR Model to Predict the COVID-19 Outbreak in Spain and Italy: Simulating Control Scenarios and Multi-Scale Epidemics. *Results in Physics*, 2021, vol. 21, article no. 103746. DOI: 10.1016/j.rinp.2020.103746.

16. Sun, J., Qi, J., Yan, Z., Li, Y., Liang, J., & Wu, S. Quantitative Study on American COVID-19 Epidemic Predictions and Scenario Simulations. *ISPRS International Journal of Geo-Information*, 2024, vol. 13, article no. 31. DOI: 10.3390/ijgi13010031.

17. Qin, X., Deng, Y., Zuo, Z., & Wang, X. Applying Reinforcement Learning to Epidemic Management: Strategic Influenza Control in Multiple Scenarios. *2022 IEEE 10th International Conference on Healthcare Informatics (ICHI)*, 2024, pp. 141–146. DOI: 10.1109/ichi61247.2024.00026.

18. Gandzha, I.S., Kliushnichenko, O.V., & Lukyanets, S.P. Modeling and Controlling the Spread of Epidemic with Various Social and Economic Scenarios. *Chaos, Solitons & Fractals*, 2021, vol. 148, article no. 111046. DOI: 10.1016/j.chaos.2021.111046.

19. Gao, S., & Wang, H. Scenario Prediction of Public Health Emergencies Using Infectious Disease Dynamics Model and Dynamic Bayes. *Future Generation Computer Systems*, 2022, vol. 127, pp. 334–346. DOI: 10.1016/j.future.2021.09.028.

20. *The Economist What Is Disease X?* Available online: https://www.economist.com/the-economist-explains/2018/03/23/what-is-disease-x (accessed on 11 February 2025).

21. Watts, D.J., & Strogatz, S.H. Collective Dynamics of "Small-World" Networks. *Nature*, 1998, vol. 393, pp. 440–442. DOI: 10.1038/30918.

22. Coulson, M. *What Is Disease X | Johns Hopkins | Bloomberg School of Public Health* Available online: https://publichealth.jhu.edu/2024/what-is-disease-x (accessed on 11 February 2025).

23. Nitzsche, C., & Simm, S. Agent-Based Modeling to Estimate the Impact of Lockdown Scenarios and Events on a Pandemic Exemplified on SARS-CoV-2. *Scientific Reports*, 2024, vol. 14, article no. 13391. DOI: 10.1038/s41598-024-63795-1.

24. Hay, M., Teichert, A., Kilz, S., & Vosen, A. Resilience in the Vaccine Supply Chain: Learning from the COVID-19 Pandemic. *Vaccines*, 2025, vol. 13, article no. 142. DOI: 10.3390/vaccines13020142.

25. Datta, A., Winkelstein, P., & Sen, S. An Agent-Based Model of Spread of a Pandemic with Validation Using COVID-19 Data from New York State. *Physica A: Statistical Mechanics and its Applications*, 2022, vol. 585, article no. 126401. DOI: 10.1016/j.physa.2021.126401.

26. Sallam, M., Kareem, N., & Alkurtas, M. The Negative Impact of Misinformation and Vaccine Conspiracy on COVID-19 Vaccine Uptake and Attitudes among the General Public in Iraq. *Preventive Medicine Reports*, 2024, vol. 43, article no. 102791. DOI: 10.1016/j.pmedr.2024.102791.

27. Masele, J.J. Misinformation and COVID-19 Vaccine Uptake Hesitancy among Frontline Workers in Tanzania: Do Demographic Variables Matter? *Human vaccines & immunotherapeutics*, 2024, vol. 20, article no. 2324527. DOI: 10.1080/21645515.2024.2324527.

28. Chatterjee, S., Bhattacharya, M., Nag, S., Dhama, K., & Chakraborty, C. A Detailed Overview of SARS-CoV-2 Omicron: Its Sub-Variants, Mutations and Pathophysiology, Clinical Characteristics, Immunological Landscape, Immune Escape, and Therapies. *Viruses*, 2023, vol. 15, article no. 167. DOI: 10.3390/v15010167.

29. Sahu, K.S., Dubin, J.A., Majowicz, S.E., Liu, S., & Morita, P.P. Revealing the Mysteries of Population Mobility amid the COVID-19 Pandemic in Canada: Comparative Analysis with Internet of Things–Based Thermostat Data and Google Mobility Insights. *JMIR Public Health and Surveillance*, 2024, vol. 10, article no. e46903. DOI: 10.2196/46903.

ISSN 1814-4225 (print)
ISSN 2663-2012 (online)

30. Liu, Y., & Rocklöv, J. The Effective Reproduction Number for the Omicron SARS-CoV-2 Variant of Concern Is Several Times Higher than Delta. *Journal of Travel Medicine*, 2022, vol. 29, article no. taac037. DOI: 10.1093/jtm/taac037.

31. Conceicao, E.P., Xu, Y., Chan, S.L., Yee, S.J., Yue, Y., Arora, S., Eng, M., Xiang, J., & Venkatachalam, I. Incubation Periods of SARS-CoV-2 Wild-Type, Delta, and Omicron Variants–Dominant Periods in Singapore. *COVID*, 2024, vol. 4, pp. 1578–1584. DOI: 10.3390/covid4100109.

32. Grewelle, R.E., & De Leo, G.A. Estimating the Infection Fatality Rate of Emerging Diseases Using a Regression Approach Applied to Global COVID-19 Cases. *Journal of Infection and Public Health*, 2025, article no. 102856. DOI: 10.1016/j.jiph.2025.102856.

33. Song, S., Madewell, Z.J., Liu, M., Miao, Y., Xiang, S., Huo, Y., Sarkar, S., Chowdhury, A., Longini, I.M., & Yang, Y. A Systematic Review and Meta-Analysis on the Effectiveness of Bivalent MRNA Booster Vaccines against Omicron Variants. *Vaccine*, 2024, vol. 42, pp. 3389–3396. DOI: 10.1016/j.vaccine.2024.04.049.

34. Teperowski M.J., Quaade, S., & Powell-Jackson, T. Supply, Then Demand? Health Expenditure, Political Leanings, Cost Obstacles to Care, and Vaccine Hesitancy Predict State-Level COVID-19 Vaccination Rates. *Vaccine*, 2022, vol. 40, pp. 6528–6548. DOI: 10.1016/j.vaccine.2022.08.050.

35. Alfredo, J., Schneider, U.V., Mollerup, S., Leineweber, T., Weis, N., Bukh, J., Pedersen, M.W., & Westh, H. SARS- CoV- 2 Spike MRNA Vaccine Sequences Circulate in Blood up to 28 Days after COVID-19 Vaccination. *Journal of Pathology, Microbiology and Immunology*, 2023, vol. 131, pp. 128–132. DOI: 10.1111/apm.13294.

36. Meng, L., Murthy, N.C., Murthy, B.P., Zell, E., Saelee, R., Irving, M., Fast, H.E., Roman, P.C., Schiller, A., Shaw, L., et al. Factors Associated with Delayed or Missed Second-Dose MRNA COVID-19 Vaccination among Persons 12 Years of Age, United States. *Emerging Infectious Diseases*, 2022, vol. 28, pp. 1633–1641. DOI: 10.3201/eid2808.220557.

37. Skafle, I., Nordahl-Hansen, A., Quintana, D.S., Wynn, R., & Gabarron, E. Misinformation about Covid-19 Vaccines on Social Media: Rapid Review. *Journal of Medical Internet Research*, 2022, vol. 24, article no. e37367. DOI: 10.2196/37367.

38. Chumachenko, D., Chumachenko, T., Kirinovych, N., Meniailov, I., Muradyan, O., Salun, O. Barriers of COVID-19 Vaccination in Ukraine during the War: The Simulation Study Using ARIMA Model. *Radioelectronic and Computer Systems*, 2022, vol. 2022, iss. 3, pp. 20–32. DOI: 10.32620/reks.2022.3.02.

39. Zhang, Y., Guo, B., Ding, Y., Liu, J., Qiu, C., Liu, S., & Yu, Z. Investigation of the Determinants for Misinformation Correction Effectiveness on Social Media during COVID-19 Pandemic. *Information Processing & Management*, 2022, vol. 59, article no. 102935. DOI: 10.1016/j.ipm.2022.102935.

40. Viana, R., Moyo, S., Amoako, D.G., Tegally, H., Scheepers, C., Althaus, C.L., Anyaneji, U.J., Bester, P.A., Boni, M.F., Chand, M., et al. Rapid Epidemic Expansion of the SARS-CoV-2 Omicron Variant in Southern Africa. *Nature*, 2022, vol. 603, pp. 679–686. DOI: 10.1038/s41586-022-04411-y.

41. Loomba, S., de Figueiredo, A., Piatek, S.J., de Graaf, K., & Larson, H.J. Measuring the Impact of COVID-19 Vaccine Misinformation on Vaccination Intent in the UK and USA. *Nature Human Behaviour*, 2021, vol. 5, pp. 337–348. DOI: 10.1038/s41562-021-01056-1.

42. Ma, J., Casadei, E., Bruce, T.J., Sepahi, A., Cain, K.D., & Salinas, I. Long-Term Efficacy of Nasal Vaccination against Enteric Red Mouth (ERM) Disease and Infectious Hematopoietic Necrosis (IHN) in Juvenile Rainbow Trout (Oncorhynchus Mykiss). *Vaccine*, 2021, vol. 40, pp. 229–238. DOI: 10.1016/j.vaccine.2021.11.077.

43. Williams, L.R., Emary, K.R.W., Phillips, D.J., Hay, J., Larwood, J.P.J., Ramasamy, M.N., Pollard, A.J., Grassly, N.C., & Voysey, M. Implementation and Adherence to Regular Asymptomatic Testing in a COVID-19 Vaccine Trial. *Vaccine*, 2024, vol. 42, article no. 126167. DOI: 10.1016/j.vaccine.2024.126167.

44. Jacobson, M., Chang, T.Y., Shah, M., Pramanik, R., & Shah, S.B. Can Financial Incentives and Other Nudges Increase COVID-19 Vaccinations among the Vaccine Hesitant? A Randomized Trial. *Vaccine*, 2022, vol. 40, pp. 6235–6242. DOI: 10.1016/j.vaccine.2022.08.060.

45. Wright, L., Steptoe, A., & Fancourt, D. Patterns of Compliance with COVID-19 Preventive Behaviours: A Latent Class Analysis of 20 000 UK Adults. *J Epidemiol Community Health*, 2021, vol. 76, pp. 247–253. DOI: 10.1136/jech-2021-216876.

46. Chu, D.K., Akl, E.A., Duda, S., Solo, K., Yaacoub, S., & Schünemann, H.J. Physical Distancing, Face Masks, and Eye Protection to Prevent Person-To-Person Transmission of SARS-CoV-2 and COVID-19: A Systematic Review and Meta-Analysis. *The Lancet*, 2020, vol. 395, pp. 1973–1987. DOI: 10.1016/S0140-6736(20)31142-9.

47. Howard, J., Huang, A., Li, Z., Tufekci, Z., Zdimal, V., van der Westhuizen, H.M., von Delft, A., Price, A., Fridman, L., Tang, L.H., et al. An Evidence Review of Face Masks against COVID-19. *Proceedings of the National Academy of Sciences*, 2021, vol. 118, article no. e2014564118. DOI: 10.1073/pnas.2014564118.

48. *CDC COVID Data Tracker*. Available online: https://covid.cdc.gov/covid-data-tracker/#datatracker-home (accessed on 11 February 2025).

49. *ECDC COVID-19 Vaccine Tracker | European Centre for Disease Prevention and Control*. Available online: https://vaccinetracker.ecdc.europa.eu/public/extensions/COVID-19/vaccine-tracker.html (accessed on 11 February 2025).

50. Johansen, R.L.R., & Tulloch, S. Using Behavioral Insights to Strengthen Strategies for Change. Practical Applications for Quality Improvement in

Healthcare. *Journal of Patient Safety*, 2024, vol. 20, pp. e78–e84. DOI: 10.1097/PTS.0000000000001242.

51. *UK Cabinet office COVID-19 Response: Living with COVID-19*. Available online: https://www.gov.uk/government/publications/covid-19-response-living-with-covid-19/covid-19-response-living-with-covid-19 (accessed on 11 February 2025).

52. Campos-Mercade, P., Meier, A.N., Schneider, F.H., Meier, S., Pope, D., & Wengström, E. Monetary Incentives Increase COVID-19 Vaccinations. *Science*, 2021, vol. 374, pp. 879–882. DOI: 10.1126/science.abm0475.

53. Dakin, J. *Supply Chain Challenges Creating Hurdles to COVID-19 Vaccine Production*. Available online: https://www.pharmtech.com/view/supply-chain-challenges-creating-hurdles-to-covid-19-vaccine-production (accessed on 11 February 2025).

54. *Vaccines Europe Vaccines Europe Reflections on Enhancing Supply Chain Resilience*. Available online: https://www.vaccineseurope.eu/wp-content/uploads/2024/09/Vaccines-Europe-reflections-on-enhancing-supply-chain-resilience_September2024.pdf (accessed on 11 February 2025).

55. King, M.L. How Manufacturing Won or Lost the COVID-19 Vaccine Race. *Vaccine*, 2024, vol. 42, pp. 1004–1012. DOI: 10.1016/j.vaccine.2023.12.031.

56. Kargar, B., MohajerAnsari, P., Esra Büyüktahtakın, İ., Jahani, H., & Talluri, S. Data-Driven Modeling for Designing a Sustainable and Efficient Vaccine Supply Chain: A COVID-19 Case Study. *Transportation Research Part E: Logistics and Transportation Review*, 2024, vol. 184, article no. 103494. DOI: 10.1016/j.tre.2024.103494.

57. Nguyen, V.H., Crépey, P., Williams, B.A., Welch, V.L., Pivette, J.M., Jones, C.H., & True, J.M. Modeling the Impact of Early Vaccination in an Influenza Pandemic in the United States. *npj Vaccines*, 2025, vol. 10, 62. DOI: 10.1038/s41541-025-01081-5.

58. *Vaccines Europe Vaccine Production Lead Times Analysis Report, Vaccines Europe Analysis of Vaccine Production Lead Times*. Available online: https://www.vaccineseurope.eu/wp-content/uploads/2023/05/Final_VE-Product-lead-time_May2023.pdf (accessed on 11 February 2025).

59. Shioda, K., Breskin, A., Harati, P., Chamberlain, A.T., Komura, T., Lopman, B.A., & Rogawski McQuade, E.T. Comparative Effectiveness of Alternative Intervals between First and Second Doses of the MRNA COVID-19 Vaccines. *Nature Communications*, 2024, vol. 15, article no. 1214. DOI: 10.1038/s41467-024-45334-8.

60. Wang, S., Zhang, F., Wang, Z., Du, Z., & Gao, C. Reproduction Numbers of SARS-CoV-2 Omicron Subvariants. *Journal of Travel Medicine*, 2022, vol. 29, article no. taac108. DOI: 10.1093/jtm/taac108.

61. Yuan, Y., Xu, J., Chen, G., Liu, Y., Ouyang, L., Ma, B., Wang, B., Yan, W., Zhang, Q., Ma, Q., et al. Comparable Immune Escape Capacity between KP.2 and Other SARS-CoV-2 Variants in the Central Chinese Population after the First COVID-19 Booster. *Scientific Reports*, 2025, vol. 15, article no. 17762. DOI: 10.1038/s41598-025-02927-7.

62. Link-Gelles, R., Chickery, S., Webber, A., Ong, T.C., Rowley, E.A.K., DeSilva, M.B., Dascomb, K., Irving, S.A., Klein, N.P., Grannis, S.J., et al. Interim Estimates of 2024–2025 COVID-19 Vaccine Effectiveness among Adults Aged ≥18 Years – VISION and IVY Networks, September 2024–January 2025. *MMWR. Morbidity and Mortality Weekly Report*, 2025, vol. 74, pp. 73–82. DOI: 10.15585/mmwr.mm7406a1.

63. Choi, T., Xie, Y., & Al-Aly, Z. Rates of Hospitalization and Death due to COVID-19 in U.S. Veterans with SARS-CoV-2 Infection in the XBB, JN.1, and KP Predominant Eras. *Open Forum Infectious Diseases*, 2025, vol. 12, article no. ofaf115. DOI: 10.1093/ofid/ofaf115.

64. Tsagkli, P., Geropeppa, M., Papadatou, I., & Spoulou, V. Hybrid Immunity against SARS-CoV-2 Variants: A Narrative Review of the Literature. *Vaccines*, 2024, vol. 12, article no. 1051. DOI: 10.3390/vaccines12091051.

65. Wu, Y., Long, Y., Wang, F., Liu, W., & Wang, Y. Emergence of SARS- CoV- 2 Omicron Variant and Strategies for Tackling the Infection. *Immunity, Inflammation and Disease*, 2022, vol. 10, article no. e733. DOI: 10.1002/iid3.733.

66. Yang, J., He, X., Shi, H., He, C., Lei, H., He, H., Yang, L., Wang, W., Shen, G., Yang, J., et al. Recombinant XBB.1.5 Boosters Induce Robust Neutralization against KP.2- and KP.3-Included JN.1 Sublineages. *Signal Transduction and Targeted Therapy*, 2025, vol. 10, article no. 47. DOI: 10.1038/s41392-025-02139-5.

67. Flaxman, S., Mishra, S., Gandy, A., Unwin, H.J.T., Mellan, T.A., Coupland, H., Whittaker, C., Zhu, H., Berah, T., Eaton, J.W., et al. Estimating the Effects of Non-Pharmaceutical Interventions on COVID-19 in Europe. *Nature*, 2020, vol. 584, pp. 257–261. DOI: 10.1038/s41586-020-2405-7.

68. Mohsenpour, A., Bozorgmehr, K., Rohleder, S., Stratil, J., & Costa, D. SARS-Cov-2 Prevalence, Transmission, Health-Related Outcomes and Control Strategies in Homeless Shelters: Systematic Review and Meta-Analysis. *EClinicalMedicine*, 2021, vol. 38, article no. 101032. DOI: 10.1016/j.eclinm.2021.101032.

69. Reed, T. *Ukraine's Health Care Infrastructure Withstands a Year of Destruction*. Available online: https://www.axios.com/2023/02/22/ukraine-war-health-care-infrastructure (accessed on 11 February 2025).

70. *UNHRC Working Group: UNHCR Operational Data Portal for the Ukraine Refugee Situation: Data Explanatory Note – Revised in June 2025*. Available online: https://data.unhcr.org/en/working-group/437?secret=unhcrrestricted&geo=0&sv=65 (accessed on 11 February 2025).

71. Rzymski, P., Falfushynska, H., & Fal, A. Vaccination of Ukrainian Refugees: Need for Urgent Action. *Clinical Infectious Diseases*, 2022, vol. 75, pp. 1103–1108. DOI: 10.1093/cid/ciac276.

ISSN 1814-4225 (print)
ISSN 2663-2012 (online)

72. Costantino, V., & MacIntyre, C.R. Impact of Vaccine Coverage and Disruption to Health Services on COVID-19 in Ukraine. *Scientific Reports*, 2024, vol. 14, article no. 14729. DOI: 10.1038/s41598-024-57447-7.

73. Pambudi, N.A., Sarifudin, A., Gandidi, I.M., & Romadhon, R. Vaccine Cold Chain Management and Cold Storage Technology to Address the Challenges of Vaccination Programs. *Energy Reports*, 2022, vol. 8, pp. 955–972. DOI: 10.1016/j.egyr.2021.12.039.

74. Petherick, A., Goldszmidt, R., Andrade, E.B., Furst, R., Hale, T., Pott, A., & Wood, A. A Worldwide Assessment of Changes in Adherence to COVID-19 Protective Behaviours and Hypothesized Pandemic Fatigue. *Nature Human Behaviour*, 2021, vol. 5, pp. 1–16. DOI: 10.1038/s41562-021-01181-x.

75. *OECD Securing Medical Supply Chains in a Post-Pandemic World*. Available online: https://www.oecd.org/en/publications/2024/02/securing-medical-supply-chains-in-a-post-pandemic-world_3c8cef7c.html (accessed on 11 February 2025).

76. Liu, Z., Zhou, J., Wang, W., Zhang, G., Xing, L., Zhang, K., Wang, Y., Xu, W., Wang, Q., Man, Q., et al. Neutralization of SARS-CoV-2 BA.2.86 and JN.1 by CF501 Adjuvant-Enhanced Immune Responses Targeting the Conserved Epitopes in Ancestral RBD. *Cell Reports Medicine*, 2024, vol. 5, article no. 101445. DOI: 10.1016/j.xcrm.2024.101445.

77. Sabahelzain, M.M., Dwyer, H., Abimbola, S., & Leask, J. Implications of Conflict on Vaccination in the Sahel Region. *BMJ Global Health*, 2025, vol. 10, article no. e016496. DOI: 10.1136/bmjgh-2024-016496.

Received 24.01.2025, Accepted 20.05.2025

ЕКСПЕРИМЕНТАЛЬНЕ ДОСЛІДЖЕННЯ ГОТОВНОСТІ ДО ХВОРОБИ Х З ВИКОРИСТАННЯМ АГЕНТНО-ОРІЄНТОВАНОГО ФРЕЙМВОРКУ ДЛЯ СЦЕНАРНОГО АНАЛІЗУ

Д. І. Чумаченко

Нові респіраторні патогени й надалі завдають суттєвих медичних і економічних збитків у світовому масштабі, що зумовлює потребу в універсальних інструментах готовності, які не опираються на специфічні дані про збудника. У цій статті досліджено, як п’ять архетипових стресорів, зростання антивакцинної дезінформації, втома від протиепідемічної поведінки, порушення постачання вакцин, поява варіанта з імунним ухиленням та руйнування інфраструктури внаслідок збройного конфлікту, змінюють перебіг гіпотетичного високонебезпечного захворювання, позначеного як Хвороба Х. Метою роботи є кількісна оцінка епідеміологічного ефекту кожного шоку в тотожній міській популяції та визначити системні вразливості, які найбільше загрожують ранньому контролю спалаху. Для досягнення цієї мети виконано послідовні завдання: проведено критичний огляд сценарно орієнтованого моделювання епідемій, розширено валідоване агентно-орієнтоване SEIRDV-ядро шляхом інтеграції динамічного поширення переконань, логістики черги доз і конфлікт-обумовленої мобільності, та здійснено серію експериментів для кожного сценарію з використанням параметрів, обґрунтованих рецензованими джерелами. Результати показують, що 15% сплеск антивакцинних переконань подвоює пікову захворюваність і додає 258 випадків смерті. 50% зниження рівня маскового режиму та дистанціювання формує вторинну хвилю, яку пізнє повторне залучення все ж скорочує на 9%. 70% дефіцит постачання мРНК-вакцини протягом 35 днів підвищує летальність на 7%. Занесення 50 випадків варіанта з R0≈9,5 та 60% втратою нейтралізації збільшує сукупну смертність на 41 % за шість тижнів. Комплексний шок, спричинений конфліктом, підвищує смертність на 71% попри 10% відтік населення. Ці нелінійні реакції виникають виключно через зміни поведінки, логістики або контексту за незмінних біологічних параметрів. Отримані результати доводять, що ефективна підготовка не може покладатися на єдиний важіль впливу. Дієва пом’якшувальна стратегія потребує синхронізованої комунікації ризиків, поетапної підтримки поведінкових інтервенцій, диверсифікованих і буферизованих виробничо-логістичних потужностей, швидкого оновлення поширення антигенів і гуманітарних коридорів для вакцинації. Запропоноване дослідження надає інструмент підтримки ухвалення рішень для стрес-тестування портфелів політик до виникнення наступного високоризикового спалаху.

Ключові слова: епідемічна модель; епідемічний процес; моделювання епідемії; моделювання; агентно-орієнтоване моделювання; місінформація; вакцинальна неохота; хвороба Х.

Чумаченко Дмитро Ігорович – канд. техн. наук, доц., доц. каф. математичного моделювання та штучного інтелекту, Національний аерокосмічний університет «Харківський авіаційний інститут», Харків, Україна; афілійований дослідник з лабораторією всюдисущих технологій охорони здоров’я, Університет Вотерлу, Вотерлу, Онтаріо, Канада; запрошений науковий співробітник, Школа міжнародних відносин Балсіллі, Вотерлу, Онтаріо, Канада.

Dmytro Chumachenko – PhD, Associate Professor, Associate Professor at the Department of Mathematical Modelling and Artificial Intelligence, National Aerospace University "Kharkiv Aviation Institute", Kharkiv, Ukraine; Research Affiliate with Ubiquitous Health Technology Lab, University of Waterloo, Waterloo, ON, Canada; Visiting Scholar, Balsillie School of International Affairs, Waterloo, ON, Canada.
e-mail: dichumachenko@gmail.com, ORCID: 0000- 0003-2623-3294.